Oxygen reduction reaction in Pr2NiO4+δ/Ce0.9Gd0.1O1.95 and La0.6Sr0.4Co0.2Fe0.8O3–δ /La0.8Sr0.2Ga0.8Mg0.2O2.80 half cells: an electrochemical study

Benoit Philippeau, Fabrice Mauvy, Clément Nicollet, Sébastien Fourcade, Jean-Claude Grenier

Oxygen reduction reaction in $Pr_2NiO_{4+\delta}/Ce_{0.9}Gd_{0.1}O_{1.95}$ and $La_{0.6}Sr_{0.4}Co_{0.2}Fe_{0.8}O_{3-\delta}/La_{0.8}Sr_{0.2}Ga_{0.8}Mg_{0.2}O_{2.80}$ half cells: an electrochemical study

Benoît Philippeau · Fabrice Mauvy · Clément Nicollet · Sébastien Fourcade · Jean Claude Grenier

Abstract The electrochemical properties of $La_{0.6}Sr_{0.4}Co_{0.2}Fe_{0.8}O_{3-\delta}$ and $Pr_2NiO_{4+\delta}$ electrodes screen-printed on $La_{0.8}Sr_{0.2}Ga_{0.8}Mg_{0.2}O_{2.8}$ and $Ce_{0.9}Gd_{0.1}O_{1.95}$, respectively, have been investigated by electrochemical impedance spectroscopy (EIS). A study of the heat treatment of $La_{0.6}Sr_{0.4}Co_{0.2}Fe_{0.8}O_{3-\delta}$ material used as oxygen electrode associated to $La_{0.8}Sr_{0.2}Ga_{0.8}Mg_{0.2}O_{2.8}$ electrolyte was performed. The $La_{0.6}Sr_{0.4}Co_{0.2}Fe_{0.8}O_{3-\delta}$ porous electrode sintered at 900 °C for 1 h in air exhibits the lowest cathodic polarization resistance; *i.e.* R_P=0.12 Ω cm^2 at 600 °C. The SEM images show that the $La_{0.6}Sr_{0.4}Co_{0.2}Fe_{0.8}O_{3-\delta}$ electrode structure is highly porous, facilitating the gas diffusion and maximizing the number of active sites for the oxygen reduction reaction (ORR). Furthermore, it forms good contact with the electrolyte after this heat treatment. In order to characterize the oxygen electrode reaction of $La_{0.6}Sr_{0.4}Co_{0.2}Fe_{0.8}O_{3-\delta}$ and $Pr_2NiO_{4+\delta}$, the electrochemical impedance spectroscopy (EIS) measurements were performed at temperatures between 400 and 700 °C and at different oxygen partial pressures (pO_2) ranging in between 10^{-3} and 0.21 atm. Analysis of the impedance data revealed that there are two different processes involved in the cathode reaction. The first process in the medium-frequency range is assigned to the oxygen surface exchange reaction at the electrode/gas interface and possibly to the ionic diffusion in the material for $La_{0.6}Sr_{0.4}Co_{0.2}Fe_{0.8}O_{3-\delta}$ and to the dissociation of the adsorbed molecular oxygen for $Pr_2NiO_{4+\delta}$. The second one at low frequency is associated to the gas phase diffusion for both cathodes. The exchange current density, i_0, allows evaluating the electrocatalytic activity of the cathode materials. The $La_{0.6}Sr_{0.4}Co_{0.2}Fe_{0.8}O_{3-\delta}/La_{0.8}Sr_{0.2}Ga_{0.8}Mg_{0.2}O_{2.8}$ couple shows the largest i_0 value, reaching 432 mA cm^{-2} at 700 °C and suggesting a high electrochemical activity for the O_2 reduction reaction.

Keywords SOFC cathode · Praseodymium nickelate · Lanthanum strontium ferro-cobaltite · AC impedance spectroscopy · Oxygen electrode reaction · Exchange current density

B. Philippeau · F. Mauvy · C. Nicollet · S. Fourcade · J. C. Grenier (✉)
CNRS, Université de Bordeaux, ICMCB, 87 Avenue du Dr. A. Schweitzer, Pessac 33608, France
e mail: grenier@icmcb bordeaux.cnrs fr

Introduction

Solid oxide fuel cells (SOFCs) are considered to be promising energy conversion devices due to their high efficiency and low pollution emissions. During the last decade, significant efforts have been devoted to lower the SOFCs operating temperature in order to decrease their overall cost and to increase their lifetime, even though it is still controversial [1–4]. To reach this goal, the use of new electrolytes with high ionic conductivity as well as the development of new cathode materials with high electrocatalytic properties is required. Among the electrolytes, gadolinium doped ceria $Ce_{0.9}Gd_{0.1}O_{1.95}$ (CGO) and strontium doped lanthanum gallate $La_{1-x}Sr_xGa_{1-y}Mg_yO_{3-\delta}$ are considered as possible alternative materials to replace the conventional yttria-stabilized zirconia (YSZ) [1, 5–9]. Concerning the cathode materials, it is now well established that mixed electronic and ionic conducting oxides are the most efficient compounds in terms of electrocatalytic properties, the oxygen reduction reaction (ORR) indeed occurring all over the surface of the particles constituting the electrode. For instance, the perovskite-type oxides, $La_{1-x}Sr_xFe_{1-y}Co_yO_{3-\delta}$ are considered as excellent cathode materials for intermediate temperature SOFCs [10–12]. More recently, a new family of oxides with K_2NiF_4-type structure, so-called Ruddlesden-Popper phases, has been investigated with regards to their

excellent mixed ionic and electronic conducting properties and to their specific structural features. For instance, the praseodymium nickelate $Pr_2NiO_{4+\delta}$ (PRN) that shows oxygen overstoichiometry seems to exhibit the best cathode performances [11–16].

In order to improve the cathode performance, it is important to identify the processes involved in the oxygen reduction reaction (ORR) mechanisms, which can be rate-limiting under operating conditions [17]. Many studies have been concerned with the $La_{1-x}Sr_xFe_{1-y}Co_yO_{3-\delta}$-based cathodes deposited on YSZ [18, 19] or CGO [20–23]. Different mechanisms have been proposed, but the understanding of the oxygen reduction reaction is still debated because of the influence of a large number of parameters, such as chemical composition, electronic and ionic conductivities, microstructural properties, operating temperature, operating atmosphere and polarization conditions.

In a recent work, the electrochemical properties of various cathode/electrolyte couples have been investigated [24]. On the basis of polarization resistance values, the couples $Pr_2NiO_{4+\delta}$/$Ce_{0.9}Gd_{0.1}O_{1.95}$ and $La_{0.6}Sr_{0.4}Fe_{0.8}Co_{0.2}O_{3-\delta}$/$La_{0.8}Sr_{0.2}Ga_{0.8}Mg_{0.2}O_{2.80}$ have been evidenced to exhibit the lowest polarization resistances, R_P, and to be suitable couples for IT-SOFC applications. They are considered in this work for further studies.

The electrochemical properties of $La_{0.6}Sr_{0.4}Co_{0.2}Fe_{0.8}O_{3-\delta}$ and $Pr_2NiO_{4+\delta}$ electrodes screen-printed on $La_{0.8}Sr_{0.2}Ga_{0.8}Mg_{0.2}O_{2.8}$ and $Ce_{0.9}Gd_{0.1}O_{1.95}$ electrolytes, respectively, are investigated. The electrochemical impedance spectroscopy (EIS) is used at various temperatures and under different oxygen partial pressures with the aim to better identify each contribution involved in the ORR. Indeed, provided the characteristic frequencies of these contributions to be different enough in the studied domain, this technique may allow deconvoluting the elementary processes and possibly identifying the rate-determining steps involved in the ORR. Such a methodology has been previously used [25–27].

Experimental

Preparation of cell components

Commercial powders were used as starting materials to prepare dense electrolyte ceramics and porous cathodes. The phase purity and the particle size distribution were checked by X-ray diffraction (XRD) and laser granulometry, respectively. Their specifications have been given in ref. [24].

In order to obtain dense electrolyte pellets, CGO ($Ce_{0.9}Gd_{0.1}O_{1.95}$) (Rhodia) and LSGM ($La_{0.8}Sr_{0.2}Ga_{0.8}Mg_{0.2}O_{2.80}$) (Sigma Aldrich) powders were isostatically pressed at 3000 bars, for 15 min, and sintered at 1400 °C for 6 h and 1450 °C for 20 h, respectively. The surface of the pellets was then roughened with sandpaper (grade 4000) to make it uniform and finally cleaned with ethanol. The obtained pellets had a diameter of ~16 mm, a thickness of ~1.5 mm and a density about 95 % of the theoretical value.

Porous electrodes were made using the screen-printing process. The LSFC ($La_{0.6}Sr_{0.4}Co_{0.2}Fe_{0.8}O_{3-\delta}$) and PRN ($Pr_2NiO_{4+\delta}$) (Marion Technologies) powders were mixed into a solvent with a commercial dispersant (terpineol) and binder (ethyl cellulose) to form inks. Depending on the used impedance spectroscopy measurement configuration (2 or 3 electrodes setup as shown in Fig. 1), working and auxiliary electrodes were deposited either on the whole or on half of the surface of both sides of the electrolyte pellets.

A specific sintering temperature was required in order to obtain a good adherence between the cathode layer and the electrolyte. The PRN/CGO couple was sintered at 1100 °C, for 1 h, in air; this temperature had been previously optimized on the basis of EIS measurements. Concerning, LSFC/LSGM half cells, different heat treatments were performed in order to select the best sintering condition on the basis of the measured polarization resistance values.

Porosity, adherence and microstructure of the symmetrical cells were determined by field emission scanning electron microscopy (SEM) using a Jeol JSM 6330 F, equipped with an EDS detector. From cross-section image of the cell, the cathode layer thickness was measured as well as the porosity calculated by means of image analysis using Image J software.

Electrochemical impedance spectroscopy measurements

In order to characterize the electrochemical properties of the electrodes, the EIS measurements were performed either in two-electrode configuration (under zero dc conditions, Fig. 1a.) or in three-electrode configuration (under dc polarization, Fig. 1b).

Two-electrode measurements:

Two-electrode impedance spectroscopy measurements were carried out using a frequency response analyser module Autolab FRA2 coupled with a potentiostat/galvanostat PGSTAT 302 N, in the range of 0.01 Hz to 1 MHz with a 50 mV signal amplitude. These measurements were performed on pellets with area A≈ 2 cm^2, under a controlled flowing gas mixture (O_2/N_2), the oxygen partial pressure ranging from 0.21 down to 10^{-3} atm, in order to determine the polarization resistance and to study the processes involved in the oxygen exchange reaction at equilibrium. The impedance data were fitted using the Zview™ software (Scribner Associates).

Three-electrode measurements:

The three-electrode cell setup was used for determining the cathodic overpotential η_C, as a function of current density i. In the schematic representation of Fig. 1b, the

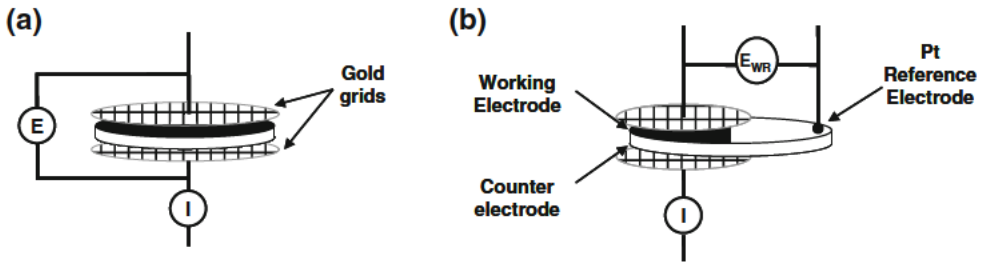

Fig. 1 Schematic representation of the two configurations used for the EIS measurements: **a** two electrode configuration and **b** three electrode setup

reference electrode is made of Pt paste deposited on the same side of the working electrode at the edge of the pellet (with $A \approx 1$ cm^2). The distance between the working and reference electrodes must be at least three times over the thickness of the electrolyte to avoid as much as possible measurement artefacts due to the influence of the current lines through the electrolyte and the reference electrode [28]. The polarization curves were obtained by voltamperometry measurements. For each point, a constant polarization voltage E_{WR} was applied between the working and the reference electrodes and the resulting current I between the working and the counter electrodes was recorded after steady state was achieved. Measurements were carried out step by step from zero dc voltage up to the highest polarization of $E_{WR}=-1$ V, then back to zero dc voltage, in order to check the reversibility. Then, the overpotential of the cathode working electrode η_C was calculated according to the following equation:

$$\eta_C = E_{WR} - R_S \times i \quad (1)$$

The ohmic drop $R_S \times i$ was deduced from the impedance diagram recorded with the 3-electrode setup at each investigated voltage step, the series resistance R_S value being obtained at the intercept of the Z' real axis at high frequencies.

Results and discussion

Electrochemical measurements under zero dc current conditions

Study of the sintering temperature of LSFC on LSGM electrolyte

With regards to the optimization of the sintering temperature achieved for the PRN/CGO couple [29], the best sintering conditions were also investigated for the LSFC cathode on LSGM electrolyte. Typical Nyquist plots recorded at 600 °C in air for LSFC/LSGM/LSFC symmetrical cells sintered at different temperatures for 1 h are given in Fig. 2. For more clarity, the value of the high-frequency resistance attributed to the LSGM electrolyte ohmic drop (R_S) was subtracted in the impedance diagram.

From the Nyquist plots, it can be observed that there are at least two semi-circles at low sintering temperatures (900 and 1000 °C), which tend to merge into one arc for higher sintering temperatures (1100 and 1150 °C).

Impedance data were fitted using an equivalent circuit constituted of one resistance R_S and two R-CPE elements in parallel associated in series as shown in Fig. 2b. In the equivalent circuit, R_S is an ohmic resistance of the cell and CPE is a constant phase element. The impedance of CPE can be expressed [30] as:

$$Z_{CPE} = \frac{1}{Y_0(j\omega)^p} \quad (2)$$

where Y_0 is the module of the CPE element, ω is the angular frequency and p is a fitting parameter between 0 and 1 related to the depression angle of the semi-circle ($p=1$ corresponds to the pure capacitance) The value of the equivalent capacitance, C_{eq}, is deduced from the relationship [30]:

$$C_{eq} = R^{\left(\frac{1-p}{p}\right)} \times Y_0^{\frac{1}{p}} \quad (3)$$

Other equivalent circuit models, involving either Gerischer or Warburg elements such as those used by Grunbaum et al. [22] and Jammik et al. [31], were no longer considered in this study because they led to divergent fits.

The polarization resistance was calculated using the relation $R_p = R_{electrode} \times A/2$; $R_{electrode}$ is the difference between low and high-frequency intercepts of the impedance diagrams with the real axis ($R_{electrode} = R_{MF} + R_{LF}$) and A, the surface area of each symmetrical electrode ($A \approx 2$ cm^2). The values of these resistances are given in Table 1. It appears that the sintering temperature has a significant effect on the electrode performances, R_p becoming larger when the sintering temperature increases. The LSFC/LSGM sample sintered at 900 °C exhibits the lowest R_p values, 0.07 Ω cm^2, 0.12 Ω cm^2 at 700 and 600 °C, respectively; these values are in the range of required targets for the development of commercial cells [32]. On the other hand, the polarization resistance is lower than the ones previously reported at 700 °C for half cells such as $La_{0.58}Sr_{0.4}Co_{0.2}Fe_{0.8}O_{3-\delta}/BaIn_{0.3}Ti_{0.7}O_{2.85}$ ($R_p \approx 0.20$ Ω cm^2), $La_{0.6}Sr_{0.4}Co_{0.2}Fe_{0.8}O_{3-\delta}/Ce_{0.8}Sm_{0.2}O_{2-\delta}$ ($R_p = 0.85$ Ω cm^2),

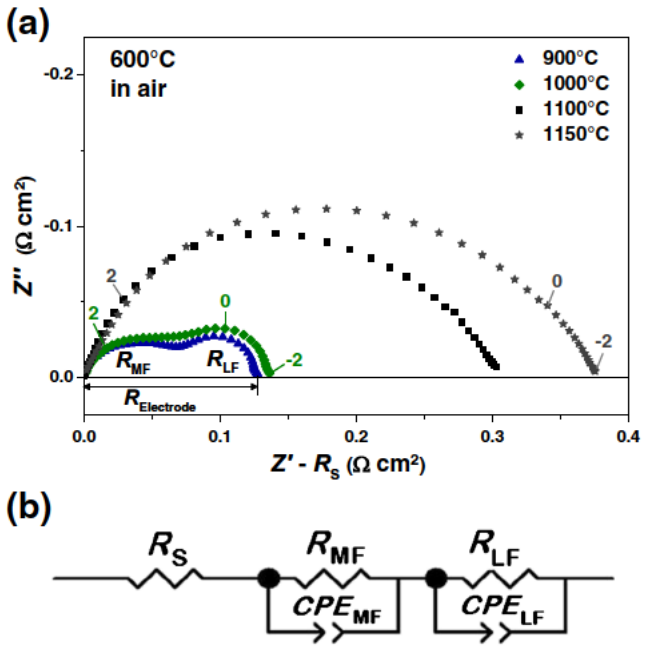

Fig. 2 **a** Typical impedance diagrams of LSFC sintered at various temperatures for 1 h on LSGM pellet and measured at 600 °C in air; **b** the equivalent circuit used for fitting AC impedance measurements

$La_{0.6}Sr_{0.4}Co_{0.2}Fe_{0.8}O_{3-\delta}/Ce_{0.9}Gd_{0.1}O_{2-\delta}$ (R_p~0.20 Ω cm^2) [33–35]. This result could be explained by the fact that the low sintering temperature is beneficial for improving the interface. The LSGM decomposition that would lead to the formation of gallates, *e.g.* $LaSrGa_3O_7$ and $Sr_4Ga_2O_7$ [36] at the interface LSFC/LSGM, having a very low conductivity, does not occur after 1 h at 900 °C, as confirmed by XRD experiments.

Then, the change in the microstructure of LSFC electrodes was studied in order to explain the effects of the sintering temperature on the R_p values. Figure 3 shows SEM images corresponding to the LSFC/LSGM interfaces after sintering at different temperatures for 1 h. It can be seen that increasing the sintering temperature leads to particle agglomeration, which decreases the electrode porosity and the number of active sites for the ORR, resulting in the increase of R_p. The porosity is estimated to be about 30 % for 900 °C/1 h against about 15 % for 1150 °C/1 h (Fig. 3d). However, all SEM images show good bonding, continuous contact at the interfaces and no delamination between electrode and electrolyte. The thicknesses of porous layers were estimated, from these observations, to be approximately 20 μm.

In the following study, the LSFC cathodes were sintered at 900 °C for 1 h, which was considered as the best sintering condition.

Study of the oxygen reduction reaction (ORR) mechanism at the cathode

In order to understand the various processes involved in the oxygen reduction reaction, a study of the influence of the oxygen partial pressure on the electrode impedance was performed at various operating temperatures (500, 600 and 700 °C). Typical impedance diagrams of the LSFC/LSGM and PRN/CGO symmetrical cells recorded at 600 °C in different gas atmospheres are given in Fig. 4a and b, respectively.

The value of the high-frequency resistance (R_s) assigned to the electrolyte was again subtracted from the total impedance. As expected, for a given temperature, this series resistance (R_s) does not significantly vary over the whole studied oxygen partial pressure range, which confirms the electrolytes to be stable under these given experimental conditions.

The best fitting of the impedance diagrams was found using two semi-circles, at middle (MF) and low frequency (LF), for all temperatures, either for LSFC or PRN electrodes. This result would suggest that the ORR involved into the LSFC and PRN electrodes can be decomposed at least into two different steps for the electrode reaction. In order to clarify this process, the experimental data were fitted using the equivalent circuit shown in Fig. 2b.

According to previous reported modelling, it is now well known that the various steps of the oxygen reduction reaction lead to different relationships between the polarization resistance and the oxygen partial pressure [37, 38].

Indeed, in steady-state conditions, the polarization resistance of each process (R_{MF} and R_{LF}) depends on the oxygen partial pressure according to the following relation:

$$R_p = R_p{}^0 \times (pO_2)^m \quad (4)$$

where the *m* value characterizes the nature of the step involved in the electrode reactions. The variation of the oxygen stoichiometry was considered to be small enough for having a

Table 1 Values of the polarization resistances measured at 600 700 °C for the LSFC electrode materials sintered on LSGM electrolyte at different temperatures

Symmetrical cell	Sintering temperature (°C/h)	Polarization resistance R_p (Ω.cm^2)	
		600 °C	700 °C
LSFC/LSGM	900 °C/1 h	0.12	0.07
	1000 °C/1 h	0.14	0.07
	1100 °C/1 h	0 30	0.08
	1150 °C/1 h	0 37	0.08

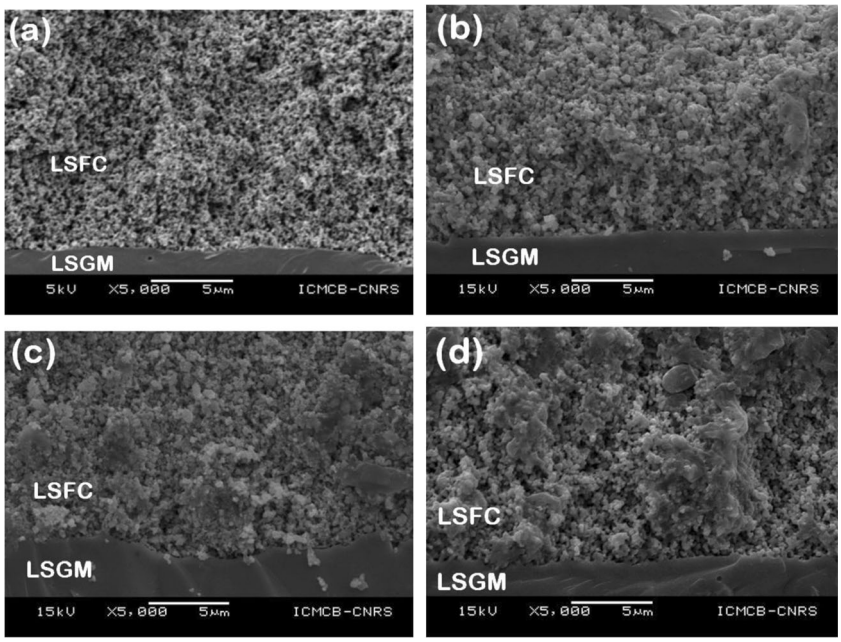

Fig. 3 SEM images of the cross section of symmetrical cells (LSFC/LSGM) sintered at 900 °C/1 h (**a**), 1000 °C/1 h (**b**), 1100 °C/1 h (**c**) and 1150 °C/1 h (**d**) after electrochemical measurements in air

negligible effect on the values of m, in agreement with most previous authors:

– m=1 characterizes the diffusion of oxygen molecules from the gas (O_2 (g)) to the active reaction sites and their adsorption at the electrode surface ($O_{2,ads}$):

$$O_2(g) \Leftrightarrow O_{2,ads} \tag{5}$$

– m=½ is related to the dissociation of the adsorbed molecular oxygen into atomic species (O_{ads}) at the electroactive sites of the mixed ionic electronic conductor (MIEC) oxide:

$$O_{2,ads} \Leftrightarrow 2\,O_{ads} \tag{6}$$

– m=¼ corresponds to the oxygen surface exchange reaction, which occurs at the two-phase gas/electrode interface; it involves the electronic transfer to the adsorbed oxygen species with the subsequent incorporation of the oxide anion into the available sites of the crystal lattice of the electrode material according to the following reaction step:

$$O_{ads} + 2\,e^{-} + V_O^{\bullet\bullet} \Leftrightarrow O_O^{x} \tag{7}$$

the oxygen vacancies being those of the MIEC oxides.

– m=0 characterizes the ionic transfer of O^{2-} oxide ions across the electrolyte-electrode interface:

$$O^{2-}_{(electrode)} \Leftrightarrow O^{2-}_{(electrolyte)} \tag{8}$$

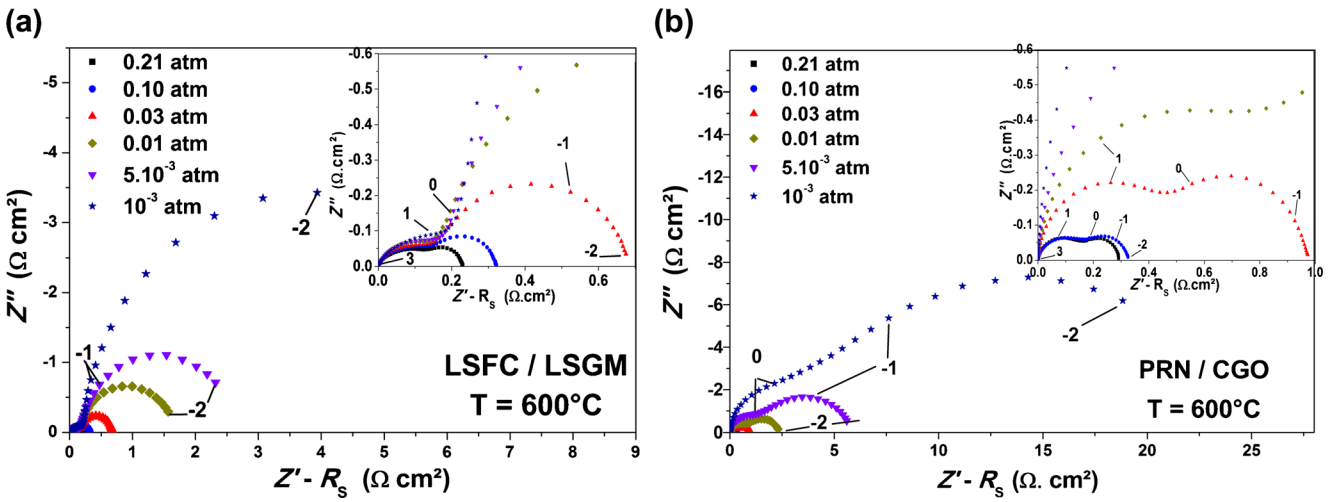

Fig. 4 Impedance diagrams recorded at 600 °C under various oxygen partial pressures for LSFC/LSGM (**a**) and PRN/CGO (**b**) half cells

The variations of the polarization resistances of each contribution (R_{MF} and R_{LF}) with pO_2 at 500, 600 and 700 °C are shown in Fig. 5a and b. Each contribution (R_{MF} and R_{LF}) and its dependences on oxygen partial pressure will be discussed separately in the following sections.

– Medium-frequency impedance (10^3-10^0 Hz)

The medium-frequency contribution was analysed with a *R//CPE* element. This equivalent sub-circuit was chosen with regards to the general features of the Nyquist plots. Although it has no real phenomenological character as a Warburg or a Gerischer element, it allows describing the complex response of an electrochemical system and determining the relaxation frequencies and the associated equivalent capacitances of each contribution. Figure 5a shows the pO_2 dependence of R_{MF} at various temperatures. Such a methodology has been previously used as observed in previous works [22, 23, 39]

For LSFC compound, R_{MF} decreases with temperature but is not significantly affected by the variation of the oxygen partial pressure. The power coefficient m is in the range of 0.10–0.04, which suggests, the rate-determining step could be assumed to be a mixed process involving both the ionic transfer across the electrolyte-electrode interface (m=0) and the oxygen surface exchange reaction (m=¼). The equivalent capacitance values, C_{MF}≈0.05–0.1 F cm $^{-2}$, are steady with temperature and nearly independent on pO_2; such values are in the range given by Adler et al. (10^{-3} to 10 F cm $^{-2}$) relative to both phenomena [20]. One should note that the thermal dependence of R_{MF} has an average activation energy value of 1.2+/−0.1 eV, which is between those found for the surface exchange coefficient, k^*, E_a=1.09 eV, and for oxygen self-diffusion coefficient, D^*, E_a=1.9 eV, reported for $La_{0.6}Sr_{0.4}Fe_{0.8}Co_{0.2}O_{3-\delta}$ [40].

Concerning the PRN compound, R_{MF} also decreases with temperature and is dependent on the oxygen partial pressure with a value of m close to ½. This dependence suggests that the dissociation of the adsorbed molecular oxygen into atomic species (Eq. 6) might be considered as the rate-determining step for this sample [41]. The capacitance values C_{MF} associated to this contribution are in the range 0.03–0.08 F cm $^{-2}$, close to those observed by Pang et al. [42].

– Low-frequency impedance (10^0–10^{-2} Hz)

The variation of the R_{LF} polarization resistances as a function of pO_2, at different temperatures, for both LSFC and PRN cathodes is shown in Fig. 5b. The n values of the slopes, around 1, together with the capacitance values C_{LF} ~0.8–4 F cm $^{-2}$, suggest that the rate-determining step is the diffusion process of O_2 molecules above and inside the porous microstructure of the electrode (Eq. 5). Furthermore, the low average activation energy values, 0.3+/−0.1 eV for LSFC and 0.2+/−0.1 eV for PRN, means a thermally nearly non-activated process, which confirms that this phenomenon is not involved in the electrode reaction kinetics. These values are in agreement with those reported by Kournoutis et al. [39] for $La_{0.8}Sr_{0.2}Co_{0.2}Fe_{0.8}O_{3-\delta}$ deposited on $Ce_{0.8}Gd_{0.2}O_{2-\delta}$ interlayer and using ZrO_2 (8 % mol Y_2O_3) electrolyte. This conclusion is also supported by the fact that the low-frequency resistance R_{LF} seems to be independent on the electrode composition at least for electrodes having the same thickness and similar microstructures and by the fact that the R_{LF} increases with decreasing pO_2.

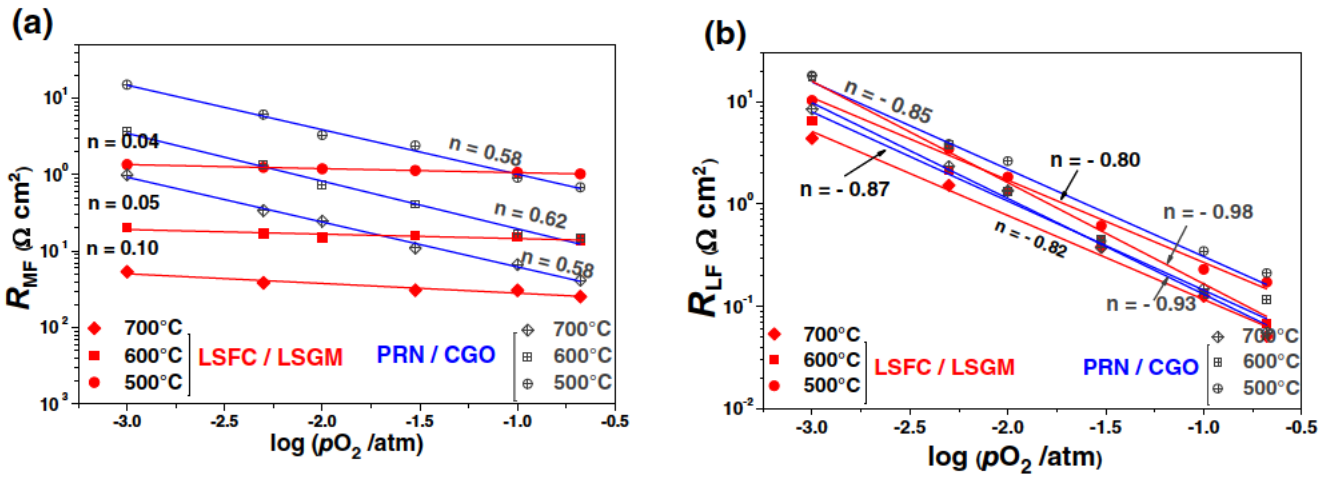

Fig. 5 Oxygen partial pressure dependences of R_{MF} (**a**) and R_{LF} (**b**) for LSFC and PRN cathodes at different temperatures

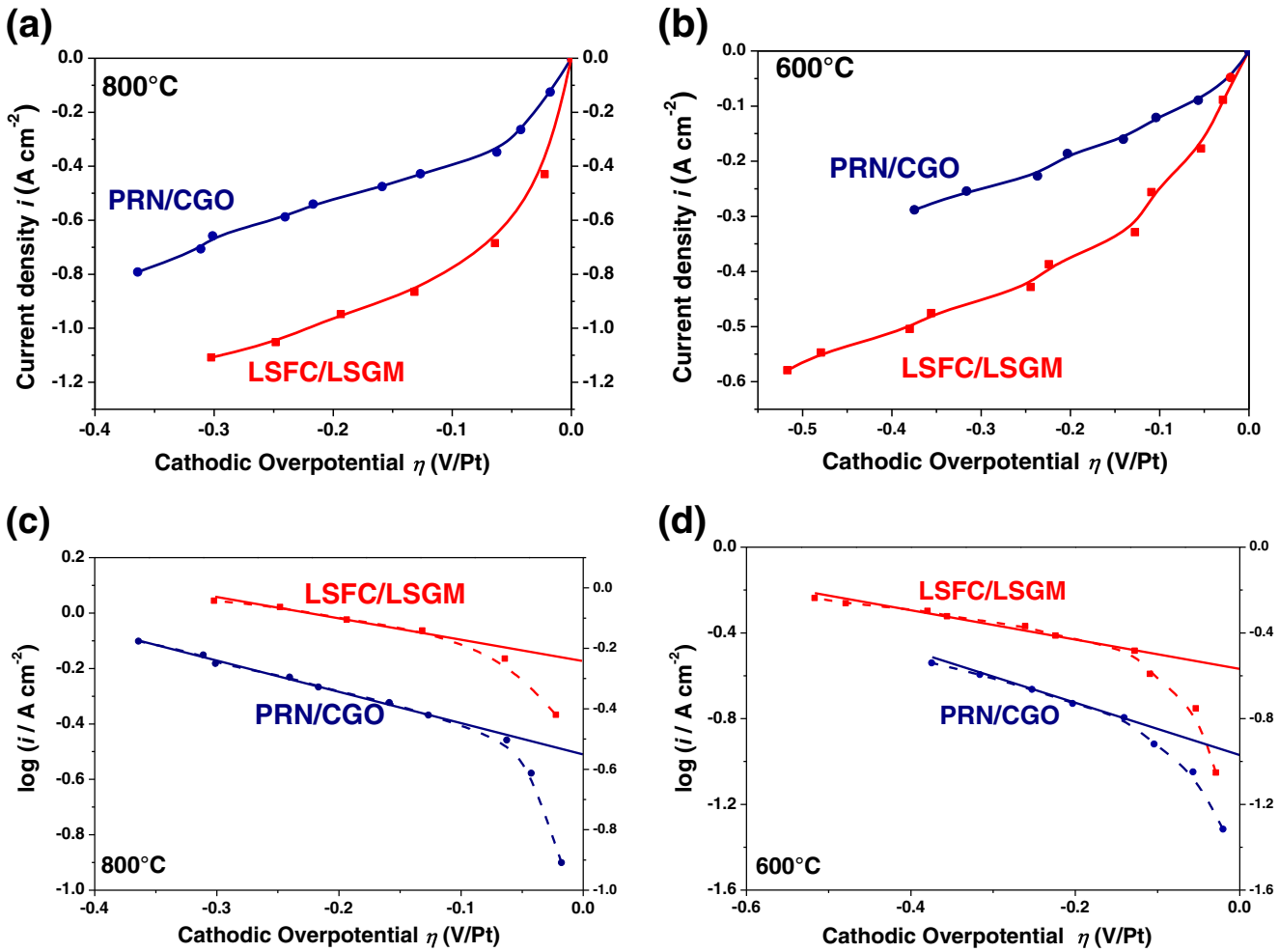

Fig. 6 Electrochemical behaviour of LSFC and PRN electrodes: cathodic polarization curves measured at 800 °C (**a**) and 600 °C (**b**) and Tafel curves measured at 800 °C (**c**) and 600 °C (**d**)

Electrochemical measurements under dc polarization

Under operating conditions, the dc polarization phenomenon at the cathode is one of the major issues of the fuel cells. In order to evaluate the performances of LSFC/LSGM and PRN/CGO half cells for SOFC applications, a cathodic dc polarization was implemented. The three-electrode configuration described in Fig.1b was used, and the cathodic polarization was measured from 500 up to 800 °C in air. The aim was to determine the cathodic overpotential as a function of the current density through the cell under steady-state conditions. The data are reported in Fig. 6 for different temperatures. At a given current density, the respective overpotentials of the LSFC and PRN cathodes decrease with temperature, indicating that the ORR kinetics are enhanced at high temperature. At each temperature, the LSFC electrode shows the lowest overpotential, whatever the current density. For instance, with the aim to compare our results with previously reported data, the overpotential η of LSFC cathode is about 5 mV under a current density of 200 mA cm ^{2} at 800 °C. This value is lower (24 mV) than the one of the PRN cathode and also much lower (27 mV) than the one of $La_{0.6}Sr_{0.4}Fe_{0.8}Co_{0.2}O_{3\ \delta}$ on $Ce_{0.8}Sm_{0.2}O_{1.9}$ [43], 45 mV for the $La_2NiO_{4+\delta}$ - $La_{0.6}Sr_{0.4}Fe_{0.8}Co_{0.2}O_{3\ \delta}$ composite electrode on $Ce_{0.8}Sm_{0.2}O_{1.9}$ electrolyte [34] and 57 mV for $La_{0.6}Sr_{0.4}Fe_{0.2}Co_{0.8}O_{3\ \delta}$ on $La_{0.9}Sr_{0.1}Ga_{0.8}Mg_{0.2}O_{3\ \delta}$ [44]. Such a good performance for the LSFC electrode reveals a high electrochemical activity of this compound for the O_2 reduction reaction, which is consistent with its low polarization resistance determined by EIS analysis.

Even if the shape of the i vs. η curves do not show a pure exponential form, the Butler-Volmer equation has been used in a empirical way to get electrode kinetics data, as it is conventionally done. This information is obtained through two parameters, the exchange current

density, i_0, and the transfer coefficient α. When the electron-transfer rate is fast and considering the range of small overpotentials, the Butler-Volmer equation can be expanded in power series. Thus, for small deviation from equilibrium, the current is approximately linear vs. η and the electrode behaves as an ohmic resistance, namely the polarization resistance R_p. Thus, in the low current density regime, the following relation can be derived from the Butler-Volmer equation [45]:

$$i_0 = \frac{RT}{nF} \times \frac{1}{R_p} \quad (9)$$

where n is the number of electrons involved in the total electrode reaction per O_2 mole (n=4), F is the Faraday constant, R is the gas constant and T is the absolute temperature.

In that case, the exchange current density i_0 values are calculated from the R_p values (obtained from the fitting data of ac impedance measurements) according to Eq. 9.

On the other hand, when the overpotential η is large enough, *i.e.* $|F\eta/RT| >> 1$, one of the exponential terms (here, the anodic one) is negligible compared with the other one. In this case, the i_0 values can be determined from the experimental i/η data obtained by linear sweep voltammetry (LSV) measurements. The i_0 values were determined from the y-intercept of the log i vs. η plot and calculated by using Eq. 10 [43]:

$$\log i = \log i_0 + \frac{a\,nF}{2.3 \times RT} \times \eta \quad (10)$$

where η is the cathodic polarization and α the charge transfer usually assumed to be 0.5.

The i_0 values calculated using AC and LSV measurements show a good agreement within the limits of experimental errors (Table 2) demonstrating the concordance of these very different measurements. In addition, the fact that the measures are carried out over 36 h, using very different polarization values (50 mV ac and up to 1 V dc) means the cathode materials are chemically stable during these experiments.

Table 2 Exchange current density vs. temperature obtained by AC Impedance and DC measurements

Electrode	T(°C)	i_0 (mA cm $^{-2}$)	
		AC	DC
LSFC	800	522+/ 120	673+/ 40
	700	318+/ 80	432+/ 15
	600	164+/ 15	270+/ 17
	500	46+/ 2	43+/ 7
PRN	800	370+/ 60	309+/ 10
	700	230+/ 25	241+/ 5
	600	102+/ 5	107+/ 8
	500	38+/ 1	35+/ 3

The i_0 values increase with increasing the operating temperature, indicating a thermally activated electrochemical reaction. Whatever the temperature, the LSFC cathode exhibits the largest i_0 values. These results suggest that the kinetics of the oxygen reduction reaction of LSFC/LSGM couple is faster than the one of PRN/CGO. At 700 °C, the i_0 value for LSFC reaches 432 mA cm $^{-2}$, which is higher than previously reported i_0 values such as 182.3 mA cm $^{-2}$ for $Ba_{0.5}Sr_{0.5}Co_{0.8}Fe_{0.2}O_{3-\delta}$/LSGM [46], 65 mA cm $^{-2}$ for LSFC/$Sm_{0.2}Ce_{0.8}O_{2-\delta}$ [43], 126 mA cm $^{-2}$ for the composite electrode LSFC/40 wt% CGO on YSZ electrolyte at the same temperature [47].

A further investigation aimed to better identify the kinetics regime of the ORR. According to the shape of the curves reported in Fig. 6, gas diffusion limitation has been considered. Indeed, the Tafel equation suggests that the current increases exponentially with increasing overpotential. However, there must be a point at which the current becomes limited by mass transport rate and log i vs. η curves begin to flatten out. The point at which this happens depends on the efficiency of gas supplying and the diffusion coefficients of electroactive species but also on the electron-transfer rate. For slow electron-transfer processes, the rate of transport is not a problem. For faster processes, the Tafel plot approach may be inadequate because, with increasing overpotential, transport limitation sets in before Tafel region is established.

The Butler-Volmer equation is a relation for current density, i as a function of overpotential η, applicable from η=0 to a value at which the influence of a limiting diffusion control becomes significant. The concept of limiting current density allows a simple derivation of the relation between the steady-state concentration

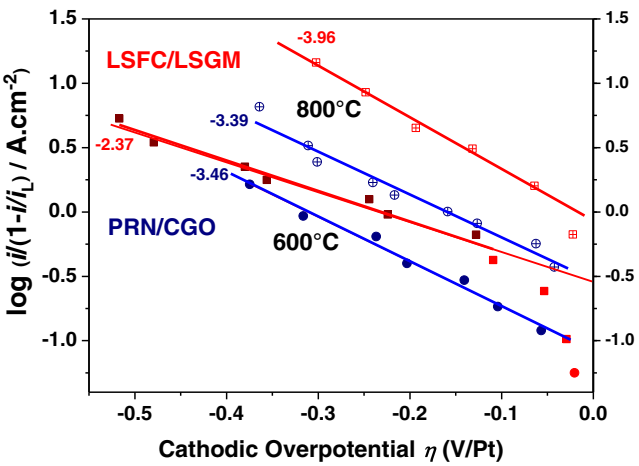

Fig. 7 Variation of log (i/(1 i/i_L)) as a function of the cathodic overpotential

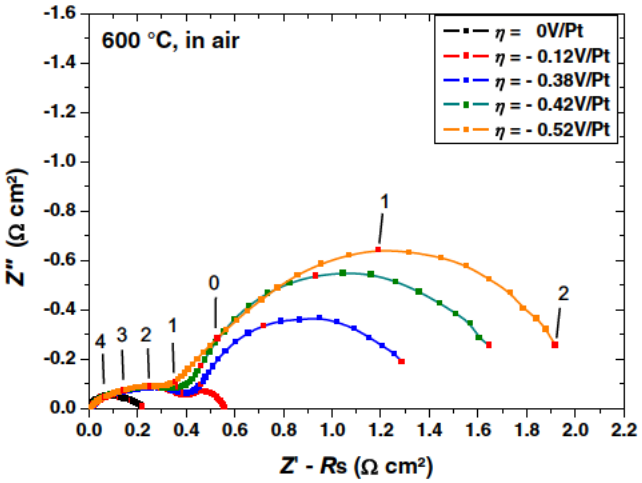

Fig. 8 EIS diagrams of LSFC/LSGM half cell for various cathodic overpotentials, under air, at 600 °C

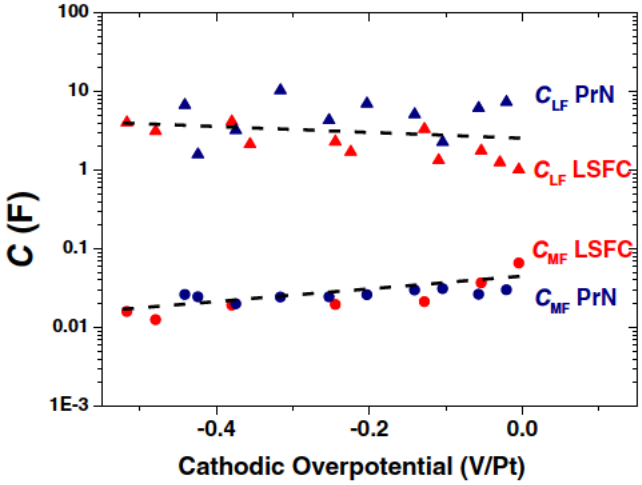

Fig. 10 MF and LF capacitances vs. cathodic overpotential for LSFC/LSGM and PrN/CGO half cells, at 600 °C, under air

overpotential η_c and the current density i if the reaction is such that other forms of overpotential are negligible. Starting from the expression of the overpotential η_c, vs. the concentration (overpotential η_c=RT/4 F×ln($C(x$=o)/$C°$), a relation between the overpotential and the limiting current density can be established: η_c=RT/4 F×ln(1-i/i_L) [48].

In order to suppress the oxygen diffusion contribution, log (i/(1-i/i_L)) vs. η graphs have been plotted in Fig. 7, the limiting current i_L being determined by extrapolation of the i vs. η plot at large overpotentials. According to these plots and especially to the values of the slope, it can be noticed that a good agreement with the theoretical Tafel slopes (4 F/RT) is obtained for both LSFC/LSGM and PRN/CGO half cells at T= 800 °C. This observation leads to suggest a mixed regime for the ORR. At large overpotentials, the ORR limiting step can be assigned to the gas diffusion process whereas at small overpotentials, it is the electron-transfer process. At 600 °C, the electrode behaviour seems to be different as the log (i/(1-i/i_L)) vs. η begins to flatten out for both LSFC/LSGM and PRN/CGO half cells, which suggests that the Tafel approach cannot be used.

The EIS diagrams recorded at 600 °C and for different overpotential values are reported in Figs. 8 and 9 for LSFC/LSGM and PRN/CGO half cells, respectively. Impedance data have been fitted using an equivalent circuit constituted of 1 resistance R_S and 2 R CPE elements in parallel associated in series. The cathodic overpotential dependences of the calculated capacitive and resistive effects are reported in Figs. 10 and 11. It clearly appears that the values of the capacitive effects associated to the medium frequencies MF and low

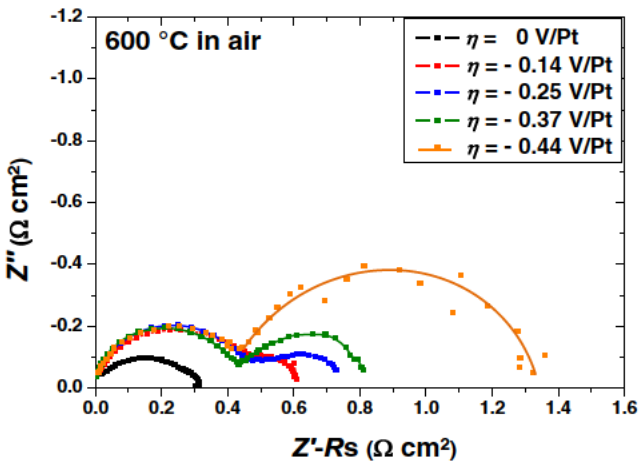

Fig. 9 EIS diagrams of PrN/CGO half cell vs. cathodic overpotential under air at 600 °C

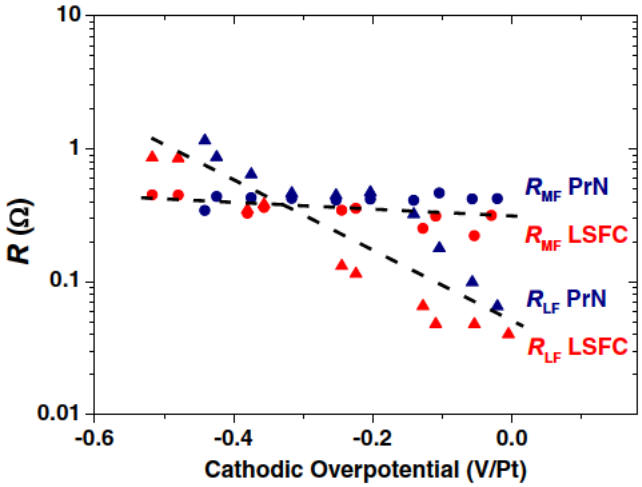

Fig. 11 MF and LF resistances vs. cathodic overpotential for LSFC/LSGM and PrN/CGO half cells, at 600 °C, under air

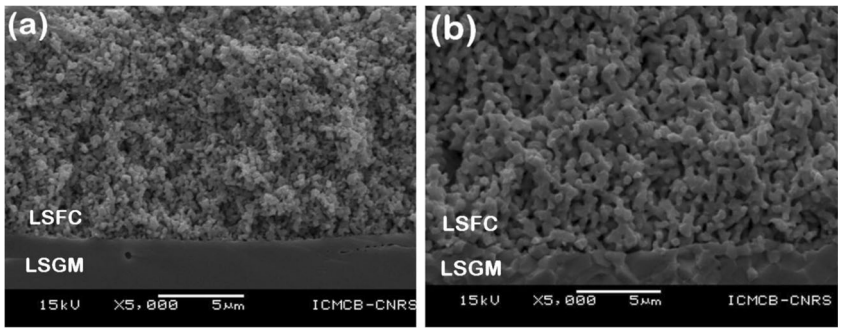

Fig. 12 SEM images of the cross section of symmetrical cells after electrochemical measurements under dc polarization in air: **a** LSFC/LSGM and **b** PRN/CGO

frequencies LF are quite constant over a large overpotential range, which supposes the various processes to be unchanged in the considered overpotential range.

The C_{LF} values are about 1 to 10 F for both half cells and characterize the gas diffusion process [26].

Concerning the MF capacitances, C_{MF}, the values are about 0.01–0.1 F for both LSFC/LSGM and PRN/CGO half cells. As reported in the literature, these contributions are assigned to the electrode process [16, 22, 26].

Regarding the MF and LF resistances, it can be observed for both LSFC/LSGM and PRN/CGO half cells that R_{MF} and R_{LF} are nearly stable vs. the cathodic overpotential whereas the R_{LF} is increasing with η. The MF resistance values are close for the two studied cells indicating that is nearly identical. These contributions have been attributed to the electrode reaction process. Concerning the LF resistances assigned to gas diffusion, this contribution is reduced in the small overpotential range and becomes the most significant in the large overpotential range. It can be deduced that the gas diffusion process is not efficient enough when the current density increases. This last contribution can be reduced by increasing the gas flow and the oxygen partial pressure of the gas supplying the electrode. Two different regimes can be identified as (i) charge transfer limitation near the equilibrium and (ii) mass transfer limitation in the large overpotential range.

In addition, from a general viewpoint, the microstructure, the adherence and the reactivity between electrode and electrolyte can drastically affect the number of active sites for the oxygen reduction process. SEM images of the LSFC and PRN electrodes have been carried out after impedance measurements under dc polarization in air. As shown in Fig. 12a, the LSFC cathode which has the highest electrocatalytic activity, shows grains with much smaller size (≈0.2 μm), about four times, than PRN (≈0.8 μm) (Fig. 12b). An increase of the grain size leads to decrease the specific surface area of the electrode and, therefore, the number of active sites. Then, it appears that the sintering of the PRN electrode leads to increase the number of necks and to decrease the specific surface area, which would explain why the PRN cathode exhibits a smaller electrochemical performance compared to LSFC cathode.

Conclusion

On the basis of previously reported results [26], two cathode/electrolyte couples were selected for further electrochemical studies: $La_{0.6}Sr_{0.4}Co_{0.2}Fe_{0.8}O_{3-\delta}$/$La_{0.8}Sr_{0.2}Ga_{0.8}Mg_{0.2}O_{2.8}$ and $Pr_2NiO_{4+\delta}$/$Ce_{0.9}Gd_{0.1}O_{1.95}$. A preliminary study of the $La_{0.6}Sr_{0.4}Co_{0.2}Fe_{0.8}O_{3-\delta}$ electrode sintering on $La_{0.8}Sr_{0.2}Ga_{0.8}Mg_{0.2}O_{2.8}$ electrolyte showed that the lowest polarization resistance (R_p=0.12 Ω cm^2 at 600 °C) is obtained after sintering at 900 °C, for 1 h. The oxygen reduction reaction for $La_{0.6}Sr_{0.4}Co_{0.2}Fe_{0.8}O_{3-\delta}$ and $Pr_2NiO_{4+\delta}$ cathodes was investigated using electrochemical impedance spectroscopy in the temperature range (500<T<700 °C) under different oxygen partial pressures ($10^{-3}<pO_2<0.21$ atm) as well as at various polarizations η (0→~−0.5 V).

EIS measurements revealed that the polarization resistance is composed of two contributions identified at medium and low frequencies. On the basis of the temperature and oxygen partial pressure dependences of the polarization resistance, the medium-frequency contribution is assigned to oxygen reduction reaction, the limiting step being dependent on the cathode material. For $La_{0.6}Sr_{0.4}Co_{0.2}Fe_{0.8}O_{3-\delta}$, it is a mixed process involving both the ionic transfer across the electrolyte-electrode interface and the oxygen surface exchange reaction, whereas for $Pr_2NiO_{4+\delta}$, it is the dissociation of the adsorbed molecular oxygen into atomic species. The low-frequency contribution is associated to the gas phase diffusion near and in the electrodes for both materials.

The highest electrocatalytic activity with regards to the oxygen reduction reaction is observed for $La_{0.6}Sr_{0.4}Co_{0.2}Fe_{0.8}O_{3-\delta}$ cathode/LSGM electrolyte, the exchange current density reaching 432 mA cm^{-2} at 700 °C.

References

1. Steele BCH, Heinzel A (2001) Materials for fuel cell technologies. Nature 414:345 352
2. Jacobson AJ (2010) Materials for solid oxide fuel cells. Chem Mater 22:660 674
3. Endler Schuck C, Leonide A, Weber A, Uhlenbruck S, Tietz F, Ivers Tiffée E (2011) Performance analysis of mixed ionic electronic conducting cathodes in anode supported cells. J Power Sources 196:7257 7262
4. Yokokawa H, Sakai N, Horita T, Yamaji K, Brito ME, Kishimoto H (2008) Thermodynamic and kinetic consider ations on degradations in solid oxide fuel cell cathodes. J Alloys Compd 452(1):41 47
5. Kharton VV, Figueiredo FM, Navarro L, Naumovich EN, Kovalevsky AV, Yaremchenko AA, Viskup AP, Carneiro A, Marques FMB, Frade JR (2001) Ceria based materials for solid oxide fuel cells. J Mater Sci 36(5):1105 1117
6. Mogensen M, Sammes NM, Tompsett GA (2000) Physical, chemical and electrochemical properties of pure and doped ceria. Solid State Ionics 129:63 94
7. Huang K, Goodenough JB (2000) A solid oxide fuel cell based on Sr and Mg doped $LaGaO_3$ electrolyte: the role of a rare earth oxide buffer. J Alloys Compd 303 304:454 464
8. Hayashi H, Suzuki M, Inaba H (2000) Thermal expansion of Sr and Mg doped $LaGaO_3$. Solid State Ionics 128:131 139
9. Ishihara T, Matsuda H, Takita Y (1994) Doped $LaGaO_3$ perovskite type oxide as a new oxide ionic conductor. J Am Chem Soc 116(9): 3801 3803
10. Wang S, Katsuki M, Dokiya M, Hashimoto T (2003) High temper ature properties of $La_{0.6}Sr_{0.4}Co_{0.8}Fe_{0.2}O_{3\ \delta}$ phase structure and elec trical conductivity. Solid State Ionics 159:71 78
11. Skinner SJ, Kilner JA (2000) Oxygen diffusion and surface exchange in $La_{2\ x}Sr_xNiO_{4+\delta}$. Solid State Ionics 135:709 712
12. Boehm E, Bassat JM, Streil MC, Dordor P, Mauvy F, Grenier JC (2003) Oxygen transport properties of $La_2Ni_{1\ x}CuxO_{4+\delta}$ mixed conducting oxides. Solid State Sci 5:973 981
13. Mauvy F, Bassat JM, Boehm E, Manaud JP, Dordor P, Grenier JC (2003) Measurement of chemical and tracer diffu sion coefficients of oxygen in $La_2Cu_{0.5}Ni_{0.5}O_{4+\delta}$. Solid State Ionics 158:395 407
14. Mauvy F, Lalanne C, Bassat JM, Grenier JC, Zhao H, Huo L, Stevens P (2006) Electrode properties of $Ln_2NiO_{4+\delta}$ (Ln=La, Nd, Pr): AC impedance and DC polarization studies. J Electrochem Soc 153: A1547 A1553
15. Escudero MJ, Aguadero A, Alonso JA, Daza L (2007) A kinetic study of oxygen reduction reaction on La_2NiO_4 cath odes by means of impedance spectroscopy. J Electroanal Chem 611:107 116
16. Ferkhi M, Ringuedé A, Khaled A, Zerroual L, Cassir M (2012) $La_{1.98}NiO_{4\pm\delta}$, a new cathode material for solid oxide fuel cell: im pedance spectroscopy study and compatibility with gadolinia doped ceria and yttria stabilized zirconia electrolytes. Electrochim Acta 75: 80 87
17. Marinha D, Dessemond L, Djurado E (2012) Electrochemical inves tigation of oxygen reduction reaction on $La_{0.6}Sr_{0.4}Co_{0.2}Fe_{0.8}O_{3\ \delta}$ cathodes deposited by electrostatic spray deposition. J Power Sources 197:80 87
18. Ringuedé A, Fouletier J (2001) Oxygen reaction on strontium doped lanthanum cobaltite dense electrodes at intermediate temperatures. Solid State Ionics 139:167 177
19. Baumann F, Fleig J, Habermeier HU, Maier J (2006) Impedance spectroscopic study on well defined (La, Sr)(Co, Fe)O3 δ model electrodes. Solid State Ionics 177: 1071 1081
20. Adler SB, Lane JA, Steele BCH (1996) Electrode kinetics of porous mixed conducting oxygen electrodes. J Electrochem Soc 143:3554 3564
21. Esquirol A, Brandon NP, Kilner JA, Mogensen M (2004) Electrochemical characterization of $La_{0.6}Sr_{0.4}Co_{0.2}Fe_{0.8}O_3$ cathodes for intermediate temperature SOFCs. J Electrochem Soc 151: A1847 A1855
22. Grunbaum N, Dessemond L, Fouletier J, Prado F, Caneiro A (2006) Electrode reaction of $Sr_{1\ x}La_xCo_{0.8}Fe_{0.2}O_{3\ \delta}$ with x =0.1 and 0.6 on $Ce_{0.9}Gd_{0.1}O_{1.95}$ at 600≤T ≤800 °C. Solid State Ionics 177:907 913
23. Grunbaum N, Dessemond L, Fouletier J, Prado F, Mogni L, Caneiro A (2009) Rate limiting steps of the porous $La_{0.6}Sr_{0.4}Co_{0.8}Fe_{0.2}O_{3\ \delta}$ electrode material. Solid State Ionics 180:1448 1452
24. Philippeau B, Mauvy F, Mazataud C, Fourcade S, Grenier JC (2013) Comparative study of electrochemical properties of mixed conducting $Ln_2NiO_{4+\delta}$ (Ln=La, Pr and Nd) and $La_{0.6}Sr_{0.4}Fe_{0.8}Co_{0.2}O_3$. Solid State Ionics 249 250:17 25
25. Adler SB (1998) Mechanism and kinetics of oxygen reduction on porous $La_{1\ x}Sr_xCoO_{3\ \delta}$ electrodes. Solid State Ionics 111:125 134
26. Jorgensen MJ, Mogensen M (2001) Impedance of solid oxide fuel cell LSM/YSZ composite cathodes. J Electrochem Soc 148(5): A433 A442
27. Jiang SP, Love JG, Ramprakash Y (2002) Electrode behaviour at (La, Sr)MnO3/Y2O3 ZrO2 interface by electrochemical impedance spec troscopy. J Power Sources 110:201 208
28. Adler SB, Henderson BT, Wilson MA, Taylor DM, Richards RE (2000) Reference electrode placement and seals in electrochemical oxygen generators. Solid State Ionics 134:35 42
29. Ferchaud C, Grenier JC, Zhang Steenwinkel Y, Van Tuel MMA, Van Berkel FPF, Bassat JM (2011) High performance praseodymium nickelate oxide cathode for low temperature solid oxide fuel cell. J Power Sources 196:1872 1879
30. Mc Donald JR (1984) Note on the parameterization of the constant phase admittance element. Solid State Ionics 13:147 149
31. Jamnik J, Maier J (2001) Generalised equivalent circuits for mass and charge transport: chemical capacitance and its implications. Phys Chem Chem Phys 3(9):1668 1678
32. SOFC Power (It), Private communication
33. Letilly M, Le Gal La Salle A, Lachgar A, Joubert O (2010) Synthesis, structural analysis and electrochemical perfor mances of BLSITCF*x* as new cathode materials for solid oxide fuel cells (SOFC) based on BIT07 electrolyte. J Power Sources 195:4779 4784
34. Zhao K, Xu Q, Huang DP, Chen M, Kim BH (2011) Electrochemical evaluation of $La_2NiO_{4+\delta}$ based composite electrodes screen printed on $Ce_{0.8}Sm_{0.2}O_{1.9}$ electrolyte. J Solid State Electrochem 16:2797 2804
35. Rembelski D, Viricelle JP, Combemale L, Rieu M (2012) Characterization and comparison of different cathode materials for SC SOFC: LSM, BSCF, SSC, and LSCF. Fuel Cells 12(2): 256 264
36. Yaremchenko AA, Shaula AL, Logvinovich DI, Kharton VV, Kovalevsky AV, Naumovich EN, Frade JR, Marques FMB (2003) Oxygen ionic conductivity of perovskite type $La_{1\ x}Sr_xGa_{1\ y}Mg_yM_{0.20}O_{3\ \delta}$ (M=Fe, Co, Ni). Math Chem Phys 82:684 690
37. Takeda Y, Kanno R, Noda M, Tomida T, Tamamoto O (1987) Cathodic polarization phenomena of perovskite electrodes with sta bilized zirconia. J Electrochem Soc 134:2656 2661
38. Siebert E, Hammouche A, Kleitz M (1995) Impedance spectroscopy analysis of $La_{1\ x}Sr_xMnO_3$ yttria stabilized zirconia electrode kinetics. Electrochim Acta 40:1741 1753
39. Kournoutis VC, Tietz F, Bebelis S (2009) AC impedance character isation of a $La_{0.8}Sr_{0.2}Co_{0.2}Fe_{0.8}O_{3\ \delta}$ electrode. Fuel Cells 9(6):852 860
40. Lane JA, Benson SJ, Waller D, Kilner JA (1999) Oxygen transport in $La_{0.6}Sr_{0.4}Co_{0.2}Fe_{0.8}O_{3\ \delta}$. Solid State Ionics 121:201 208

41. Mogni L, Grunbaum N, Prado F, Caneiro A (2011) Oxygen reduction reaction on Ruddlesden popper phases studied by impedance spec troscopy. J Electrochem Soc 158(2):B202 B207
42. Pang S, Jiang X, Li X, Wang Q, Su Z (2012) Characterization of Ba deficient $PrBa_{1-x}Co_2O_{5+\delta}$ as cathode material for intermediate tem perature solid oxide fuel cells. J Power Sources 204:53 59
43. Liu J, Co AC, Paulson S, Birss VI (2006) Oxygen reduction at sol gel derived $La_{0.8}Sr_{0.2}Co_{0.8}Fe_{0.2}O_3$ cathodes. Solid State Ionics 177:377 387
44. Guo W, Liu J, Jin C, Gao H, Zhang Y (2009) Electrochemical evalu ation of $La_{0.6}Sr_{0.4}Co_{0.8}Fe_{0.2}O_{3-\delta}$ $La_{0.9}Sr_{0.1}Ga_{0.8}Mg_{0.2}O_{3-\delta}$ composite cathodes for La0.9Sr0.1Ga0.8Mg0.2O3 δ electrolyte SOFCs. J Alloys Compd 473:43 47
45. Piao J, Sun K, Zhang N, Chen X, Xu S, Zhou D (2007) Preparation and characterization of $Pr_{1-x}Sr_xFeO_3$ cathode material for intermedi ate temperature solid oxide fuel cells. J Power Sources 172:633 640
46. Liu B, Zhang Y, Zhang L (2009) Oxygen reduction mechanism at $Ba_{0.5}Sr_{0.5}Co_{0.8}Fe_{0.2}O_{3-\delta}$ cathode for solid oxide fuel cell. Int J Hydrogen Energy 34:1008 1014
47. Qiang F, Sun KN, Zhang NQ, Zhu XD, Le S, Zhou DR (2007) Characterization of electrical properties of GDC doped A site defi cient LSCF based composite cathode using impedance spectroscopy. J Power Sources 168(2):338 345
48. J Wiley & Sons Inc. Publ. (1980) Electrochemical methods. Fundamentals and applications